ACS APPLIED MATERIALS & INTERFACES

Research Article

www.acsami.org

# General One-Pot Template-Free Hydrothermal Method to Metal Oxide Hollow Spheres and Their Photocatalytic Activities and Lithium Storage Properties

Di Li, Qing Qin, Xiaochuan Duan, Jiaqin Yang, Wei Guo, and Wenjun Zheng*

Department of Materials Chemistry, Key Laboratory of Advanced Energy Materials Chemistry (MOE), and TKL of Metal and Molecule-Based Material Chemistry, College of Chemistry, Nankai University, 94 Weijin Road, Tianjin 300071, People's Republic of China

Supporting Information

**ABSTRACT:** A general and facile one-pot template-free hydrothermal strategy has been developed to synthesize various metal oxide ($TiO_2$, $SnO_2$ and $\alpha$-$Fe_2O_3$) hollow spheres with unified morphologies. The formation of hollow structure involves a trifluoroacetic acid (TFA)-assisted Ostwald ripening process. Photocatalytic activities of the as-prepared $TiO_2$ product are evaluated by the photodegradation of Rhodamine B (RhB), which the $TiO_2$ hollow spheres obtained from 450 °C thermal treatment exhibit higher photocatalytic activity than Degussa P25. In addition, electrochemical measurements demonstrate that all of the as-prepared metal oxides hollow spheres have the potential applications in lithium-ion battery. We have a great expectation that this synthesis strategy can afford a new universal route for functional metal oxide hollow materials preparation without using template.

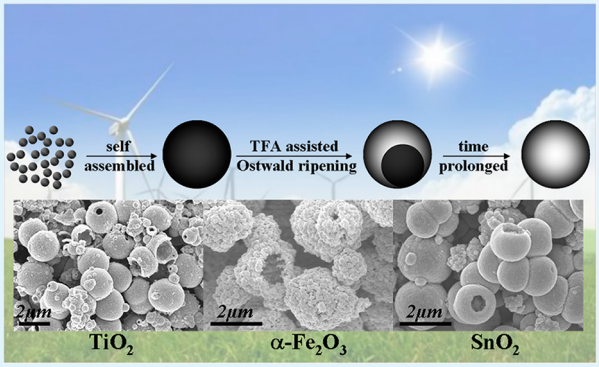


**KEYWORDS:** *general method, template-free, hollow structure, Ostwald ripening process, photocatalytic avtivity, lithium ion battery*

## 1. INTRODUCTION

Hollow structures with nanometer or micrometer size have been strongly motivated because of their unique properties of low effective density, high specific surface area, and good permeation.[1−4] In particular, metal oxide hollow structures with excellent optical, electrical and magnetic properties, have attracted more attentions owing to their numerous potential applications in biosensors,[5,6] catalysis,[7−9] lithium-ion battery,[10−14] delivery system,[15] solar cells,[16] and so on. In recent years, various chemical routes have been developed for manufacturing metal oxide hollow structures, such as template-assisted method[17−23] involving hard template (silica spheres, polymer latex, and carbon) and soft template (emulsion micelles/droplets, gas bubble) and template-free strategy[24−31] including the Ostwald ripening process, Kirkendall effect, or chemically induced self-transformation. Generally, the template-assisted method is considered as a powerful general way to prepare hollow structures via a sacrificing materials route.[32,33] Unfortunately, it usually needs postprocess to remove the template, which not only consume lots of time and energy but also may introduce heterogeneous impurities. More importantly, the hollow structures may then lose many of their active sites as a result of surface reconstruction. For this regard, it is well-understood that significant attention has been directed toward to template-free method and great achievements have been obtained in the past decade. Lou et al.[34] reported a simple, economical, and environmentally benign method to synthesize 3D hierarchical urchinlike $\alpha$-FeOOH hollow spheres via a glycerol-assisted one-pot reaction. In particular, this synthsis route neither involved any surfactant nor toxic materials. Yang et al.[35] synthesis of CuO hollow spheres with hierarchical pores and structure by a simple one-pot template-free method which is merely used $CuSO_4$, KOH, and $NH_3{\cdot}H_2O$ aqueous solution at 68 °C. However, the template-free methods are usually just suitable for certain specific metal oxide hollow structures, and no clear evidence can indicate that it can be applied to general metal oxides. Therefore, this is still a big challenge to fabricate metal oxide hollow structures by a general and facile route.

In this paper, we report a general one-pot template-free hydrothermal strategy for preparation of $TiO_2$, $\alpha$-$Fe_2O_3$ and $SnO_2$ hollow spheres. The formation mechanism of the hollow structures may be described as a TFA assisted Ostwald ripening process. Moreover, we have investigated that the photocatalytic activities and lithium-ion storage properties of the as-prepared hollow structures, which demonstrated that the $TiO_2$ sample

Received: June 21, 2013
Accepted: August 22, 2013
Published: August 22, 2013

   dx.doi.org/10.1021/am4024059 | ACS Appl. Mater. Interfaces 2013, 5, 9095−9100

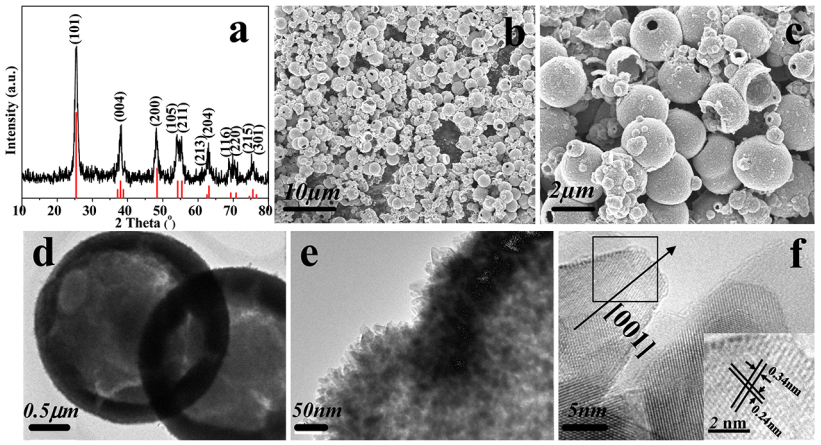


**Figure 1.** (a) XRD pattern of as-prepared $TiO_2$ hollow spheres (black) and standard XRD pattern of anatase $TiO_2$ (JCPDS card, no. 21−1272) (red), (b, c) SEM images and (d−f) TEM and HRTEM images of the as-synthesized $TiO_2$ derived from hydrothermal reaction. Inset shows the corresponding lattice fringe matching the distance between (101) planes of anatase crystals.

with 450 °C calcination showed a higher photocatalytic activity than commercial Degussa P25, and all of the as-prepared metal oxide hollow structures exhibited a potential application in lithium storage. This work for the first time realizes that the fabrication of various functional metal oxides hollow spheres using a general template-free method, which may open up a new opportunity for preparation of metal oxide hollow structures.

## 2. EXPERIMENTAL SECTION

**Synthesis of Metal Oxide Hollow Spheres.** In a typical synthesis, $TiO_2$ hollow spheres procedure, a homogeneous solution including 17 mL of $H_2O$, 4.7 mL of N, N-dimethylformamide (DMF) and 2.3 mL of TFA was dropped to 2 mmol of titanium butoxide (TBOT) in a Teflon-lined autoclave. The temperature of the autoclave was raised to 180 °C and held this temperature for 24 h. The white precipitates obtained were collected by centrifugation and washed with deionized water and ethanol several times to remove dissolved impurities. The products were dried in a vacuum oven at 60 °C.

The fabrication methods for $\alpha$-$Fe_2O_3$ and $SnO_2$ hollow spheres were similar to prepare $TiO_2$ just change TBOT to iron chloride hexahydrate ($FeCl_3 \cdot 6H_2O$) or tin chloride pentahydrate ($SnCl_4 \cdot 5H_2O$), and prolonged the reaction time to 48 h when fabricated $SnO_2$, while other parameters kept constant.

**Photocatalytic Reactions.** The photocatalytic activities of the as-prepared $TiO_2$ hollow spheres were evaluated by the photocatalytic degradation of RhB aqueous solution at room temperature under UV light irradiation. A 300 W Hg arc lamp was used as a light source to provide the ultraviolet light. In a typical reaction, 0.1 g of as-prepared photocatalysts was dispersed into 100 mL of RhB aqueous solution ($1 \times 10^{-5}$ M). Before light irradiating, the suspension was stirred for 30 min in the dark to reach adsorption equilibrium of RhB on the surface of hollow spheres. Then, the reaction was stopped at 30 min intervals and 10 mL of reaction solutions were extracted to determine the concentrations of the aqueous RhB solution by UV/vis spectroscopy. In this study, P25 was used as a reference catalyst to photocatalytic RhB under the same condition as the as-prepared samples. RhB aqueous solution without photocatalysts irradiated by UV light was used as a blank experiment and the as-prepared photocatalysts reacting with RhB in dark were used as comparative evaluation.

**Material Characterization.** X-ray diffraction (XRD) patterns of the samples were recorded on a Bruker D8 Focus diffractometer (CuK$\alpha$ radiation, $\lambda$ = 1.5418 Å, 40 kV), field emission scanning electron microscopy (FESEM) measurement was performed by JSM-6700F instrument operated at an accelerating voltage of 10 kV, transmission electron microscope (TEM) and high-resolution transmission electron microscope (HRTEM) using Tecnai G2 instrument at an accelerating voltage of 200 kV, the Brunauer−Emmett−Teller (BET) specific surface area ($S_{BET}$) of the sample was analyzed by nitrogen adsorption in a Tristar 3000 nitrogen adsorption apparatus, UV spectra were recorded on a Cary 5000 spectrometer at room temperature.

**Electrochemical Measurements.** The electrochemical measurements were examined using 2025 coin cells with 1 M LiPF6 electrolyte solution dissolved in a mixture of ethylene carbonate (EC)/dimethyl carbonate (DMC) (v/v% = 1:1) solution as the counter/reference electrode electrolyte, and Celgard 2400 membranes as the separator. The working electrodes were prepared by mixing 80 wt % active material ($TiO_2$, $SnO_2$ and $\alpha$-$Fe_2O_3$ hollow spheres), 10 wt % acetylene black (Super-P), and 10 wt % polyvinylidene fluoride (PVDF) binder dissolved in N-methyl-2-pyrrolidinone (NMP) and the mixture was stirred for 24 h at room temperature to form homogeneous slurry. Then, the slurry was uniformly coated on a copper foil, and dried at 80 °C for 24 h under vacuum. Galvanostatic charge−discharge cycles were performed by LAND CT2001A electrochemical workstation at a constant current density of 100 mA $g^{-1}$ in the potential range from 1.0 to 3.0 V for $TiO_2$, 0.001 to 2.5 V for $SnO_2$ and 0.05 to 3.0 for $\alpha$-$Fe_2O_3$ at room temperature.

## 3. RESULTS AND DISCUSSIONS

In a typical hydrothermal synthesis procedure, with hydrolysis of TOBT in the TFA and DMF mixed aqueous solution, $TiO_2$ hollow spheres with a diameter of about 2 $\mu$m can be obtained. Pure anatase phase and well-crystallized $TiO_2$ have been confirmed by XRD. All diffraction peaks can be indexed to anatase (JCPDS card, no. 21−1272) with lattice constants $a$ = 0.3785 nm, $b$ = 0.3785 nm, and $c$ = 0.9514 nm and no impurities can be detected. Based on the Scherrer equation, the average particle size was calculated to be 46 nm. As shown in SEM images in Figure 1, the obtained hollow spheres exhibit thin and coarse shell with a large cavity space which can be observed from the fragment. Most of the hollow spheres shells have a hole, which may be caused by collision during the period of hydrothermal reaction or the step of ultrasonic dispersion. The bright and dark contrast of TEM images further confirms the results of SEM characterization. Furthermore, TEM and HRTEM images in Figure 1 also demonstrate that the shells of the hollow spheres are random assembled by numerous small single crystal truncated bipyramid units with lattice spacing of 0.34 and 0.24 nm, corresponding to (101) and (004) planes, respectively, which reveals that the units grow along the [001] axis and are consisted by {001} and {101} facets. The $N_2$

adsorption−desorption isotherms for the post-treatment $TiO_2$ hollow spheres (see Figure S1a in the Supporting Information) was characteristic of a type IV isotherm with a type H1 hysteresis loop according to Brunauer-Deming-Deming-Teller (BDDT) classification, which indicates by a hysteresis loop at high relatively pressures associated with capillary condensation of gases within mesopores in the size range of 2−50 nm.[36] The BET surface area is 108.35 $m^2$ $g^{-1}$. The pore size distribution (see Figure S1b in the Supporting Information) calculated from desorption branch of the nitrogen isotherm by the BJH method shows a range from 2 to 20 nm with 11.88 nm as center.[37]

To investigate the formation mechanism of the hollow spheres, we monitored a detailed time-dependent evolution process. TEM images in Figure 2 show that the products were

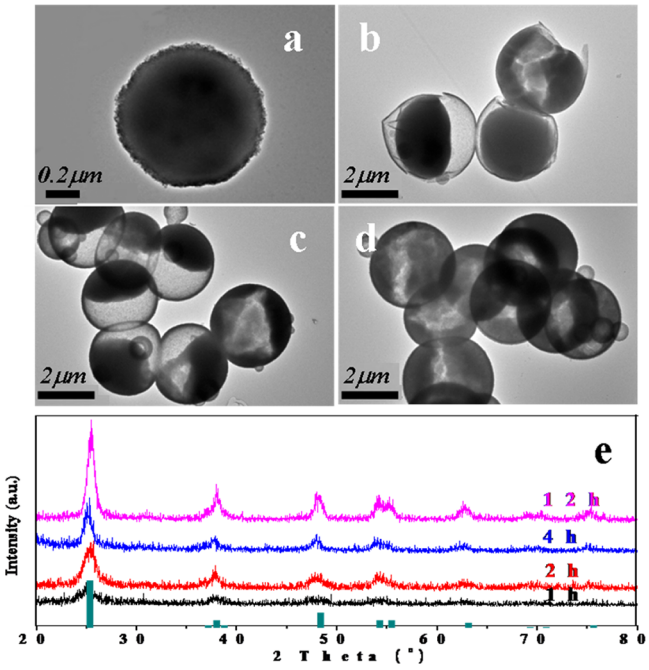


**Figure 2.** TEM images of $TiO_2$ samples synthesized for (a) 1, (b) 2, (c) 4, and (d) 12 h, respectively, and corresponding XRD patterns (e) (green line in e is standard XRD pattern of anatase $TiO_2$). Other reaction parameters are kept constant.

obtained at different growth stages. At the first 1 h, solid spheres with a diameter of 1 μm were obtained, while there is no sign for hollowing. The dark contrast of TEM image reveals that when the reaction time was prolonged to 2 h, with a size swelling, core−shell structure which consisted by an irregular shape core and a sphere shell was formed. With a longer process of 4 h, the diameter of the shell nearly unchanged, but the core of the core−shell structure diminished and the shell part thickened gradually. Upon prolonging reaction time to 12 h, core−shell structure disappeared and hollow spheres formed. SEM images also further confirm the above results. As shown in Figure S2 in the Supporting Information, with the reaction time prolonged, the hollowing process was quite obviously and the wall of the hollow sphere was gradually thin. The corresponding XRD patterns reveal that all of the samples prepared at different reaction time are anatase phase, and no phase transition takes place during the whole reaction process, indicating that the core−shell structures are homogeneous. The crystallinities of the products increase and the sizes of the nanogranule units grow larger gradually with prolonged the reaction time, which can be confirmed by the peak height and peak width of XRD patterns.

On the basis of the above results, a possible mechanism for the formation of $TiO_2$ hollow spheres has been illustrated in Scheme 1. At the very beginning, for reducing the high surface

**Scheme 1. Schematic Illustration of the Possible Process for the Formation of Hollow Spheres**

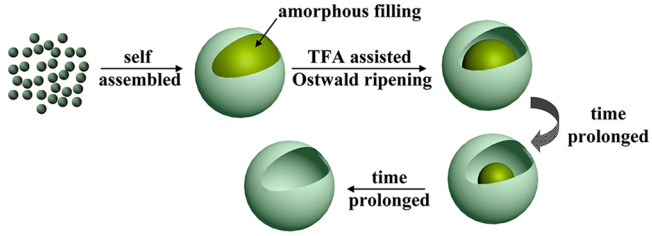


energy associated with unsatisfied bonds, freshly formed crystalline nanoparticles spontaneous self-organized by adjacent particles in a common crystallographic orientation and joined these particles at a planar interface to form numerous poorly crystallized $TiO_2$ solid spheres.[38,39] Furthermore, a mass of hydrogen-bonds such as N−H, O−H, F−H bonds constructed between the DMF (containing N, O atoms)/TFA (containing 3 F atoms) and the $TiO_2$ nanogranules with a lot of hydroxyl on surface encouraged subcrystals interconnecting using DMF/TFA as mediums.[40,41] Under the strong polar solvent of DMF and high reaction temperature, TFA might be decomposed weakly to HF, which can dissolve $TiO_2$ particles.[42] Because of the faster nucleation rate and the production of more crystallites with smaller sizes, which was induced by the initial high supersaturation, the crystallites located in the inner cores had a smaller size and higher curvature than the crystallites located in the outer surface. As a result, the crystallites located in the inner cores were easier to dissolve than the exteriors nanoparticles, and the exteriors nanoparticles could serve as the new starting sites for the subsequent recrystallization process and continued crystal growth.[43] Therefore, solid spheres transformed to a homogeneous core−shell structure. Until the interior nanoparticles dissolved completely, hollow spheres could be obtained with a swelled size and better crystallinity. The hollowing process is corresponds to the classical theory of Ostwald ripening, which involves "the growth of large crystals from those of smaller size which have a higher solubility than the larger ones".[44] To further verify the effects of TFA and DMF in the formation of hollow structure, a series of control experiments were carried out. First, when either TFA or DMF was replaced by $H_2O$, both of the obtained products were composed by irregular small nanogranules (see Figure S3 in the Supporting Information), which indicated that self-organizion can not appear when absent enough hydrogen-bond mediums afforded by reaction solution. Moreover, using other acids (methanoic acid, acetic acid, malonic acid, benzoic acid, citric acid, sulfuric acid) to instead of TFA, no hollow structure could be found. Most of the products composed by nanogranules except that using citric acid, sulfuric acid. Though the $TiO_2$ subcrystals could self-organize under the existence of citric acid and sulfuric acid, there was not enough corrosivity of the acid to bring about the hollowing process (see Figure S4 in the Supporting Information).

To demonstrate the potential applicability of the as-prepared $TiO_2$ hollow spheres for the removal of organic pollutions from


dx.doi.org/10.1021/am4024059 | ACS Appl. Mater. Interfaces 2013, 5, 9095−9100

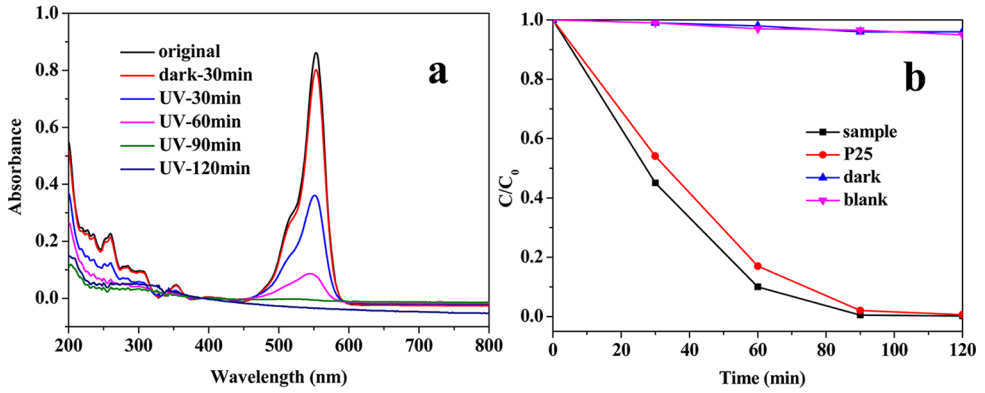


**Figure 3.** (a) Absorption spectra of a solution of RhB in the presence of $TiO_2$ hollow spheres and under exposure to UV light, (b) time course of the decrease in the dye concentration using different catalysts.

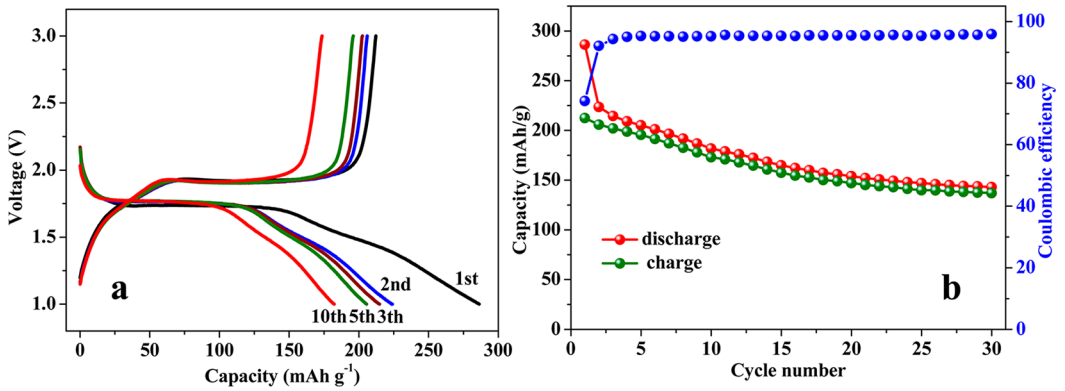


**Figure 4.** Electrochemical properties of $TiO_2$ hollow spheres: (a) galvanostatic discharge/charge voltage curves (current density = 100 mA $g^{-1}$); (b) cycling performance and Coulombic efficiency over 30 cycles (current density = 100 mA $g^{-1}$).

wastewater, we investigated their photocatalytic activities by employing the photocatalytic degradation of RhB under UV light, where Degussa P25 $TiO_2$ was used as a reference photocatalyst. The $TiO_2$ sample were calcined at 450 °C for 3 h and then cooled to room temperature before being used as a photocatalyst. After calcining, the morphology, BET surface area, and pore size distribution of the $TiO_2$ hollow structure are not obviously altered and it still kept in the anatase phase (see Figure S5 in the Supporting Information). As shown in Figure 3a, with the increasing illumination time, the main absorption peak (about 550 nm) vanishes gradually and completely disappears after about 90 min. During the photocatalytic period, the main absorption peak position has almost no change and no other absorption band appears, which suggest that the whole process was dominated by photocatalytic degradation mode other than dye sensitization.

Time course of the decrease in the dye concentration using different catalysts is shown in Figure 3b, where all of the reaction time was deducted the time of adsorption equilibrium. Compared with P25, the as-prepared hollow spheres photocatalysts exhibits better photocatalytic activity. After UV light irradiation 30 min, RhB is degraded by 60% over as-prepared photocatalyst, completely degraded under the irradiation of UV light for 90 min. Both only irradiation without photocatalyst and only photocatalyst without irradiation lead to little degradation of RhB. The excellent photocatalytic activity of the as-prepared $TiO_2$ hollow spheres is mainly contributed by both of the relative higher BET surface area and more active sites provided by truncated bipyramid shape units than P25 photocatalyst.[45]

Anatase $TiO_2$ has been intensively investigated as a host structure for reversible lithium insertion/extraction. The following equation represents electrochemical reaction between $Li^+$ and anatase $TiO_2$ in a $TiO_2$/Li half cell

$$TiO_2 + \chi Li + \chi e^- \leftrightarrow Li_\chi TiO_2 \quad (1)$$

where the maximum insertion coefficient $x$ is determined to be ~0.5,[46] which leads to a theoretical lithium storage capacity of 167.5 mA h $g^{-1}$.[2] The electrochemical performance of the as-prepared $TiO_2$ hollow spheres were evaluated by galvanostatic charge/discharge cycling at a current density of 100 mA $g^{-1}$ (see Figure 4). The first discharge and charge capacities are 286.3 and 212.2 mA h $g^{-1}$, respectively, leading to an initial Coulombic efficiency is 74%. Considering that the theoretical capacity of bulk $TiO_2$, the capacity of the $TiO_2$ hollow spheres is extraordinarily high, which exhibits a unique property of nanostructured materials. The increased specific-charging capacity of the initial cycle is mostly attributed to the small particle size and the formation of solid−electrolyte interface.[47] In the second cycle, the discharge and charge capacities decreases to 223.6 and 205.9 mA h $g^{-1}$, respectively, leading to a much higher Coulumbic efficiency of 92%, which indicates that the irreversible capacity loss decreases because of the trapping of lithium ion inside the $TiO_2$ framework.[48] In addition, even after the tenth charge process, the discharge and charge capacities still sustains 181.7 mA h $g^{-1}$ and 173 mA h $g^{-1}$, which is higher than the theoretical capacity of $TiO_2$. The

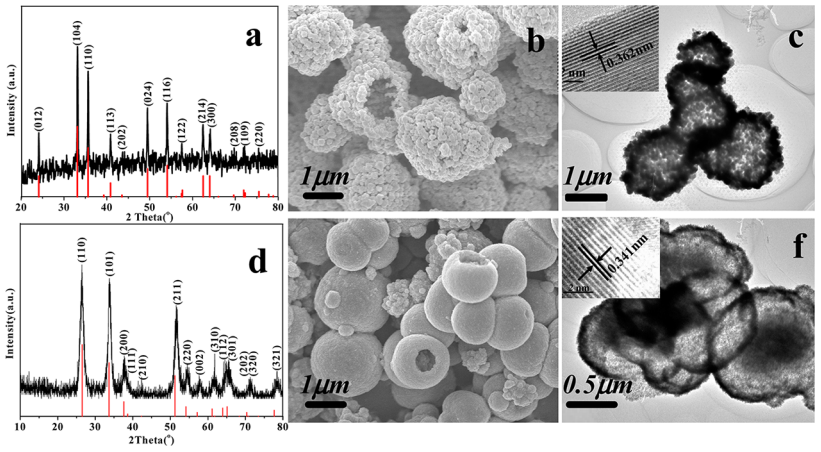


**Figure 5.** XRD patterns, SEM, TEM, and HRTEM images for the as-prepared hollow spheres: (a–c) $\alpha$-$Fe_2O_3$ and (d–f) $SnO_2$, respectively. The red lines in a and d are the standard XRD patterns of rhombohedral phase $\alpha$-$Fe_2O_3$ (JCPDS 33–0664) and tetragonal phase $SnO_2$ (JCPDS 41–1445).

high capacity is mainly attributed to the abundance of active surface sites for lithium storage of hollow spheres.[49] A capacity of ~150 mA h $g^{-1}$ is retained after 30 cycles of discharge and charge indicated the good cycling stability of the $TiO_2$ hollow spheres.

According to the above result and subsequent analysis, we further put forward an idea: whether this synthesis strategy can be used to fabricate other metal oxides which have the potential to form hollow spheres via Ostwald ripening process? With this idea, we use $FeCl_3 \cdot 6H_2O$ and $SnCl_4 \cdot 5H_2O$ to replace TBOT as the metal sources for synthesis of metal oxide while other parameters maintained constant except changing the reaction time. Interestingly, $\alpha$-$Fe_2O_3$ and $SnO_2$ microsized hollow spheres have been obtained successfully. Figure 5 shows XRD patterns, SEM, TEM and HRTEM images of as-prepared $\alpha$-$Fe_2O_3$ and $SnO_2$ hollow spheres. XRD patterns (Figure 5a, d) indicate that both samples are pure-phase and the diffraction lines are identified rhombohedral phase $\alpha$-$Fe_2O_3$ (JCPDS 33–0664) and tetragonal phase $SnO_2$ (JCPDS 41–1445). The sharp peaks with high intensity indicate the well crystallinity of the samples. The structures and morphologies of the as-prepared hollow spheres are characterized by SEM and TEM images. As shown in Figure 5b, c, e, and f, the $\alpha$-$Fe_2O_3$ hollow spheres with an average diameter of 2 $\mu$m are composed of numerous polygon nanogranules units with a size of ~200 nm. Because of the large size of the nanocrystal units, the surface of the $\alpha$-$Fe_2O_3$ hollow spheres is much more coarse, whereas the morphology of $SnO_2$ is similar to $TiO_2$. The HRTEM images (insert in Figure 5c, f) indicate that the lattice fringes with a spacing of 0.362 and 0.341 nm are assigned to stable $\alpha$-$Fe_2O_3$ (012) and $SnO_2$ (110), respectively. The time-dependent evolutions of $\alpha$-$Fe_2O_3$ and $SnO_2$ are also investigated and the detailed characterization results are illustrated in Figure S6–S9 in the Supporting Information. The BET surface areas of as-prepared $\alpha$-$Fe_2O_3$ and $SnO_2$ are 4.16 and 108.25 $m^2$ $g^{-1}$, and the average pore sizes are 65.77 and 6.04 nm (see Figure S1b, c in the Supporting Information), respectively. Obvious Ostwald ripening processes of both metal oxides can be observed from the TEM images. The only distinct difference is the $\alpha$-$Fe_2O_3$ hollowing process start from the center while the $TiO_2$ and $SnO_2$ hollowing process first occur in the region underneath the inner surface of the solid spheres. The primary reason may be related to the $\alpha$-$Fe_2O_3$ solid spheres were much looser than others which is convenient for TFA to enter the center of the spheres.[50] Therefore, the center of the $\alpha$-$Fe_2O_3$ solid spheres will be first dissolved and no process of core–shell structure could be found.

We also investigated the lithium storage properties of the as-prepared $SnO_2$ and $\alpha$-$Fe_2O_3$ hollow spheres (see Figure S10 in the Supporting Information). The electrochemical reaction mechanisms of Li with $SnO_2$ and $\alpha$-$Fe_2O_3$ in Li-ion batteries can be described as

$$SnO_2 + 4Li^+ + 4e^- \rightarrow Sn + 2Li_2O \quad (2)$$

$$Sn + \chi Li^+ + \chi e^- \leftrightarrow Li_\chi Sn (0 \le \chi \le 4.4) \quad (3)$$

$$\alpha - Fe_2O_3 + \chi Li^+ + \chi e^- \leftrightarrow \alpha - Li_\chi Fe_2O_3 (0 \le \chi \le 6) \quad (4)$$

and the theoretical capacity of $SnO_2$ and $\alpha$-$Fe_2O_3$ are 1494[51] and 1007 mA h $g^{-1}$,[52] respectively. The first discharge and charge capacities are 1764.3 and 779.9 mA h $g^{-1}$ for $SnO_2$ and 1062.8 mA h $g^{-1}$ and 590.2 mA h $g^{-1}$ for $\alpha$-$Fe_2O_3$. Compared to the theoretical capacities of $SnO_2$ and $\alpha$-$Fe_2O_3$, both of the hollow structures exhibited higher discharge capacities, which is as same as the as-prepared $TiO_2$ hollow spheres. After 10 cycles, the as-prepared $SnO_2$ hollow spheres still exhibits very high discharge and charge capacities of 724.4 and 692.3 mAh $g^{-1}$, respectively. Furthermore, its Coulombic efficiency maintained at ~95.6%. Although the discharge and charge capacities of $\alpha$-$Fe_2O_3$ hollow spheres decreases with increasing cycles (derived from the relative larger particle size), its Coulombic efficiency increases to higher than 98%.

## 4. CONCLUSION

In summary, a general and facile template-free hydrothermal method for synthesis of metal oxides hollow spheres has been reported. On the basis of the experimental results, a TFA assisted Ostwald ripening process has been proposed as the possible mechanism for the formation of hollow structures. The hollow nature and self-assemble form of the as-prepared $TiO_2$ hollow spheres provide a relative higher BET surface area and more active catalytic sites than P25 photocatalyst, which leading to an excellent photocatalytic activity under UV light irradiation. When the hollow structures ($TiO_2$, $SnO_2$ and $\alpha$-$Fe_2O_3$) were employed as lithium battery electrodes, they exhibited extraordinarily high first discharge and charge capacities and Coulombic efficiency. We believe that the

hollow spheres synthesized using this method has considerable potential as photocatalysts and electrode materials for lithium ion batteries.

## ■ ASSOCIATED CONTENT

### Supporting Information

Nitrogen adsorption−desorption isotherms and the corresponding pore size distributions of the as-prepared samples, SEM images of $TiO_2$ samples synthesized without adding TFA or DMF, SEM images of $TiO_2$ samples synthesized using other acids, characterization (SEM, XRD, nitrogen adsorption) of $TiO_2$ hollow spheres after calcination, SEM images of all metal oxides and TEM images of $\alpha$-$Fe_2O_3$ and $SnO_2$ prepared for different time and electrochemical properties of as-prepared $SnO_2$ and $\alpha$-$Fe_2O_3$ hollow spheres. This material is available free of charge via the Internet at http://pubs.acs.org/.

## ■ AUTHOR INFORMATION

### Corresponding Author

*E-mail: zhwj@nankai.edu.cn.

### Funding

### Notes

The authors declare no competing financial interest.

## ■ ACKNOWLEDGMENTS

We thank the National Natural of Science Foundation of China (Grants 20971070, 21073095 and 21371101) and the 111 project (B12015) for the support of this work.

## ■ REFERENCES

(1) Yin, L. W.; Bando, Y.; Li, M. S.; Golberg, D. *Small* **2005**, *1*, 1094−1099.
(2) Wang, W. S.; Zhen, L.; Xu, C. Y.; Shao, W. Z. *J. Phys. Chem. C* **2008**, *112*, 14360−14366.
(3) Zhou, L.; Zhao, D. Y.; Lou, X. W. *Adv. Mater.* **2012**, *24*, 745−748.
(4) Joo, J. B.; Zhang, Q.; Lee, I.; Dahl, M.; Zaera, F.; Yin, Y. D. *Adv. Funct. Mater.* **2012**, *22*, 166−174.
(5) Zhu, H. T.; Wang, J. X.; Xu, G. Y. *Cryst. Growth Des.* **2009**, *9*, 633−638.
(6) Han, L. J.; Liu, R. J.; Li, C. S.; Li, H. H.; Li, C. X.; Zhang, G. J.; Yao, J. N. *J. Mater. Chem.* **2012**, *22*, 17079−17085.
(7) Zeng, Y.; Wang, X.; Wang, H.; Dong, Y.; Ma, Y.; Yao, J. N. *Chem. Commun.* **2010**, *46*, 4312−4314.
(8) Zhang, H. J.; Du, G. D.; Lu, W. Q.; Cheng, L. L.; Zhu, X. D.; Jiao, Z. *CrystEngComm* **2012**, *14*, 3793−3801.
(9) Xi, G. C.; Yan, Y.; Ma, Q.; Li, J. F.; Yang, H. F.; Lu, X. J.; Wang, C. *Chem.—Eur. J.* **2012**, *18*, 13949−13953.
(10) Wang, B.; Chen, J. S.; Wu, H. B.; Wang, Z. Y.; Lou, X. W. *J. Am. Chem. Soc.* **2011**, *133*, 17146−17148.
(11) Yao, Y.; McDowell, M. T.; Ryu, I.; Wu, H.; Liu, N.; Hu, L. B.; Nix, W. D.; Cui, Y. *Nano Lett.* **2011**, *11*, 2949−2954.
(12) Jin, L.; Xu, L. P.; Morein, C.; Chen, C. H.; Lai, M.; Dharmarathna, S.; Dobley, A.; Suib, S. L. *Adv. Funct. Mater.* **2010**, *22*, 3373−3382.
(13) Wu, H. B.; Chen, J. S.; Hng, H. H.; Lou, X. W. *Nanoscale* **2012**, *4*, 2526−2542.
(14) Chen, J. S.; Lou, X. W. *Small* **2013**, *9*, 1877−1893.
(15) Chen, Y.; Chen, H. R.; Zeng, D. P.; Tian, Y. B.; Chen, F.; Feng, J. W.; Shi, J. L. *ACS nano* **2010**, *4*, 6001−6013.
(16) Wu, D. P.; Zhu, F.; Li, J. M.; Dong, H.; Li, Q.; Jiang, K.; Xu, D. S. *J. Mater. Chem.* **2012**, *22*, 11665−11671.
(17) Lou, X. W.; Archer, L. A. *Adv. Mater.* **2008**, *20*, 1853−1858.
(18) Du, N.; Zhang, H.; Chen, J.; Sun, J. Y.; Chen, B. D.; Yang, D. R. *J. Phys. Chem. B* **2008**, *112*, 14836−14842.
(19) Wang, X.; Liao, M. Y.; Zhong, Y. T.; Zheng, J. Y.; Tian, W.; Zhai, T. Y.; Zhi, C. Y.; Ma, Y.; Yao, J. N.; Bando, Y.; Golberg, D. *Adv. Mater.* **2012**, *24*, 3421−3425.
(20) Lai, X. Y.; Li, J.; Korgel, B. A.; Dong, Z. H.; Li, Z. M.; Su, F. B.; Du, J.; Wang, D. *Angew. Chem.* **2011**, *123*, 2790−2793.
(21) Zhang, G. Q.; Yu, L.; Wu, H. B.; Hoster, H. E.; Lou, X. W. *Adv. Mater.* **2012**, *24*, 4609−4613.
(22) Kao, K. C.; Tsou, C. J.; Mou, C. Y. *Chem. Commun.* **2012**, *48*, 3454−3456.
(23) Cheng, S.; Yan, D.; Chen, J. T.; Zhuo, R. F.; Feng, J. J.; Li, H. J.; Feng, H. T.; Yan, P. X. *J. Phys. Chem. C* **2009**, *113*, 13630−13635.
(24) Li, J.; Zeng, H. C. *J. Am. Chem. Soc.* **2007**, *129*, 15839−15847.
(25) Zhu, L. P.; Xiao, H. M.; Zhang, W. D.; Yang, G.; Fu, S. Y. *Cryst. Growth Des.* **2008**, *8*, 957−963.
(26) Liu, Y.; Li, Q.; Gao, S. A.; Shang, J. K. *J. Am. Ceram. Soc.* **2013**, *96*, 1421−1427.
(27) Pan, A. Q.; Wu, H. B.; Yu, L.; Lou, X. W. *Angew. Chem., Int. Ed.* **2013**, *52*, 2226−2230.
(28) Wang, H. Q; Miyauchi, M.; Ishikawa, Y.; Pyatenko, A.; Koshizaki, N.; Li, Y.; Li, L.; Li, X. Y.; Bando, Y.; Golberg, D. *J. Am. Chem. Soc.* **2011**, *133*, 19102−19109.
(29) Xiang, Q. J.; Yu, J. G.; Cheng, B.; Ong, H. C. *Chem. Asian J.* **2010**, *5*, 1466−1474.
(30) Lou, X. W.; Wang, Y.; Yuan, C. L.; Lee, J. Y.; Archer, L. A. *Adv. Mater.* **2006**, *18*, 2325−2329.
(31) Li, L. L.; Chu, Y.; Liu, Y.; Dong, L. H. *J. Phys. Chem. C* **2007**, *111*, 2123−2127.
(32) Peng, Q.; Xu, S.; Zhuang, Z. B.; Wang, X.; Li, Y. D. *Small* **2005**, *1*, 216−221.
(33) Sun, X. M.; Liu, J. F.; Li, Y. D. *Chem.—Eur. J.* **2006**, *12*, 2039−2047.
(34) Wang, B.; Wu, H. B.; Yu, L.; Xu, R.; Lim, T. T.; Lou, X. W. *Adv. Mater.* **2012**, *24*, 1111−1116.
(35) Qin, Y.; Zhang, F.; Chen, Y.; Zhou, Y. J.; Li, J.; Zhu, A. W.; Luo, Y. P.; Tian, Y.; Yang, J. H. *J. Phys. Chem. C* **2012**, *116*, 11994−12000.
(36) Yu, J. G.; Wang, G. H.; Cheng, B.; Zhou, M. H. *Appl. Catal., B* **2007**, *69*, 171−180.
(37) Yu, J. G.; Fan, J. J.; Lv, K. L. *Nanoscale* **2010**, *2*, 2144−2149.
(38) Penn, R. L.; Banfied, J. F. *Science* **1998**, *281*, 969−971.
(39) Jia, B. P.; Gao, L. *J. Phys. Chem. C* **2008**, *112*, 666−671.
(40) Zhou, J. K.; Lv, L.; Yu, J. Q.; Li, H. L.; Guo, P. Z.; Sun, H.; Zhao, X. S. *J. Phys. Chem. C* **2008**, *112*, 5316−5321.
(41) Ho, S. Y.; Wong, A. S. W.; Ho, G. W. *Cryst. Growth Des.* **2009**, *9*, 732−736.
(42) Yang, H. G.; Zeng, H. C. *J. Phys. Chem. B* **2004**, *108*, 3492−3495.
(43) Yu, X. X.; Yu, J. G.; Cheng, B.; Huang, B. B. *Chem.—Eur. J.* **2009**, *15*, 6731−6739.
(44) Ostwald, W. Z. *Phys. Chem.* **1897**, *22*, 289−295.
(45) Joo, J. B.; Lee, I.; Dahl, M.; Moon, G. D.; Zaera, F.; Yin, Y. D. *Adv. Funct. Mater.* **2013**, DOI: 10.1002/adfm.201300255.
(46) Lindström, H.; Södergren, S.; Solbrand, A.; Rensmo, H.; Hjelm, J.; Hagfeldt, A.; Lindquist, S. E. *J. Phys. Chem. B* **1997**, *101*, 7717−7722.
(47) Li, N. C.; Martin, C. R. *J. Electrochem. Soc.* **2001**, *148*, 164−170.
(48) Das, S. K.; Darmakolla, S.; Bhattacharyya, A. J. *J. Mater. Chem.* **2010**, *20*, 1600−1606.
(49) Chen, J. S.; Tan, Y. L.; Li, C. M.; Cheah, Y. L.; Luan, D.; Madhavi, S.; Boey, F. Y. C.; Archer, L. A.; Lou, X. W. *J. Am. Chem. Soc.* **2010**, *132*, 6124−6130.
(50) Yu, J. G.; Zhang, J. *Dalton Trans.* **2010**, *39*, 5860−5867.
(51) Zhou, X. S.; Wan, L. J.; Guo, Y. G. *Adv. Mater.* **2013**, *25*, 2152−2157.
(52) Xu, X. D.; Cao, R. G.; Jeong, S.; Cho, J. *Nano Lett.* **2012**, *12*, 4988−4991.